A Traditional Approach for Color Constancy and Color Assimilation Illusions with Its Applications to Low-Light Image Enhancement

Oguzhan Ulucan[1*], Diclehan Ulucan[1] and Marc Ebner[1]

[1*]Computer Science, University of Greifswald, Walther-Rathenau-Str., Greifswald, 17489, Mecklenburg-Vorpommern, Germany.

*Corresponding author(s). E-mail(s): oguzhan.ulucan@uni-greifswald.de;
Contributing authors: diclehan.ulucan@uni-greifswald.de;
marc.ebner@uni-greifswald.de;

Abstract

The human visual system achieves color constancy, allowing consistent color perception under varying environmental contexts, while also being deceived by color illusions, where contextual information affects our perception. Despite the close relationship between color constancy and color illusions, and their potential benefits to the field, both phenomena are rarely studied together in computer vision. In this study, we present the benefits of considering color illusions in the field of computer vision. Particularly, we introduce a learning-free method, namely *multiresolution color constancy*, which combines insights from computational neuroscience and computer vision to address both phenomena within a single framework. Our approach performs color constancy in both multi- and single-illuminant scenarios, while it is also deceived by assimilation illusions. Additionally, we extend our method to low-light image enhancement, thus, demonstrate its usability across different computer vision tasks. Through comprehensive experiments on color constancy, we show the effectiveness of our method in multi-illuminant and single-illuminant scenarios. Furthermore, we compare our method with state-of-the-art learning-based models on low-light image enhancement, where it shows competitive performance. This work presents the first method that integrates color constancy, color illusions, and low-light image enhancement in a single and explainable framework.

Keywords: Computational Color Constancy, Color Assimilation Illusions, Low-light Image Enhancement, Multiresolution Color Constancy

Fig. 1 Example color assimilation illusion (Bach Last accessed: 01.04.2025). We perceive the colors of the target region in the color assimilation illusion as orangish and purplish although its reflectance is red which can be easily identified when the context is removed.

1 Introduction

Our visual system is evolved in a way that it can perceive distances, adapt our vision to low-light environments, and differentiate between colors by discounting the effects of the environmental context unconsciously (Zeki 1993). Especially, the last ability is interesting when we consider the fact that color is not a physical property of objects but rather the result of complex mechanisms of the human visual system (Zeki 1993). For instance, when we enter a room illuminated by a yellowish light source we can easily recognize the true color of a red apple as red instead of yellow. This ability, called *color constancy*, is usually referred to as a phenomenon since the neural mechanisms underlying it are not yet fully understood even though they have been widely studied for decades (Zeki 1993; Gegenfurtner 1999; Brainard and Radonjic 2004; Ebner 2007; Hurlbert 2007). However, in certain situations, the environmental context can mislead our visual system, causing the colors we perceive to differ significantly from the object's actual physical reflectance. One of the notable examples deceiving our visual system is the phenomenon called *color assimilation illusions* (Fig. 1). In these illusions, the colors of the target region's local neighbors, i.e., context, affect our perception so that the colors of the target region shift towards that of its local neighbors. This emphasizes that local features, that is, the average color of a scene, are key attributes of our perception (Linnell and Foster 1997; Gegenfurtner 2003).

Even though we can perform color constancy, our perception is deceived by color illusions. On the other hand, machine vision systems can easily determine the actual colors of the illusions, yet they cannot perform color constancy without further computations. Machine vision systems need *computational color constancy* to identify the true colors of objects under different colored light sources since the captured image is a result of the interaction between the camera sensors' response and the illuminant of the scene, e.g., without computational color constancy, a white object illuminated by yellowish light would be captured as yellow (Ulucan et al. 2024c). Thus, computational color constancy allows us to work with accurate reflectance values. The algorithms that are developed in the field of color constancy are helpful in the area of digital photography and also for various computer vision tasks such as object detection, and object classification (Ebner 2007).

Color constancy is not only studied in computer vision, but it is also extensively investigated alongside color illusions in computational neuroscience (Shapiro et al. 2018; Gegenfurtner 1999). Even though both fields acknowledge the strong link between these two

This version of the article has been accepted for publication, after peer review (when applicable) but is not the Version of Record and does not reflect post-acceptance improvements, or any corrections. The Version of Record is available online at: http://dx.doi.org/10.1007/s11263-025-02595-0

visual phenomena (Marini and Rizzi 2000; Corney and Lotto 2007; Gomez-Villa et al. 2019; Ulucan et al. 2024b), their motivations for investigating them differ. In computational neuroscience, both concepts serve as beneficial tools to investigate the underlying mechanisms of human visual information processing (Marini and Rizzi 1997, 2000; Blakeslee and McCourt 2004; Zeman et al. 2015; Mitra et al. 2018; Corney and Lotto 2007; Hirsch and Tal 2020; Kubota et al. 2021; Gomez-Villa et al. 2022). Despite the extensive research in this field, we still do not know how the human visual system performs color constancy while being deceived by color illusions. A deeper understanding of the neural mechanisms would lead to a more accurate model of human color perception (Gomez-Villa et al. 2025). This might lead to an explainable model that, in turn, could enable significant advancements in computer vision applications and digital photography, particularly for algorithms inspired by the capabilities of the human visual system. However, despite the potential benefits of investigating these phenomena together, it is quite surprising that in computer vision, they are rarely studied simultaneously (Gomez-Villa et al. 2019; Ulucan et al. 2024b, 2022a). Motivated by the lack of research in this field, we began investigating color illusions from the perspective of computational color constancy for the first time in computer vision. In our studies, we demonstrated that indeed, these illusions can provide valuable cues for enhancing the performance of color constancy methods (Ulucan et al. 2024b, 2022a). The results of our studies motivated us to develop a single framework that can address both phenomena simultaneously, whose importance is highlighted in computational neuroscience studies (Corney and Lotto 2007). Therefore, in our recent study, we developed a learning-free method, which is the first computational color constancy algorithm that can address both visual phenomena with a single approach, without focusing on developing a method explicitly for one phenomenon or the other (Ulucan et al. 2024a). While developing our method, we combined the best of both worlds by considering the observations from computational neuroscience and building on the white-balancing experience of computer vision. In short, we designed a method that purely relies on low-level processing, utilizing scale-space computations and space average color. Moreover, in our comprehensive experiments, we demonstrated that our learning-free method can achieve competitive results when compared with state-of-the-art models on different multi-illuminant color constancy benchmarks. These results highlight the importance of taking inspiration from the human visual system and classical computer vision methods to develop simple and explainable algorithms that can compete or even surpass learning-based approaches.

In this study, we extend our previous work (Ulucan et al. 2024a) by offering new discussions and experiments on additional datasets, specifically single-illuminant benchmarks, to demonstrate that our method performs effectively not only in multi-illuminant cases but also in single-illuminant scenarios. Furthermore, we slightly modify our method to test it for a new application, low-light image enhancement (Ulucan et al. 2025). With this extension, we present the generalizability of our approach in both different illumination settings and distinct computer vision tasks.

Overall, this paper highlights the following contributions:

- We introduce the first computational color constancy method that addresses both color constancy and color illusions within a single framework by integrating insights from computational neuroscience and computer vision.

- We propose a learning-free method that purely relies on low-level processing, including scale-space computations and the modified version of the local space average color method.
- We present that our method is effective not only in multi-illuminant cases but also in single-illuminant scenarios, thereby we show its applicability across various lighting conditions.
- We apply our method to the task of low-light image enhancement and evaluate its performance on two widely used benchmarks, comparing it against 22 learning-based methods. This demonstrates its effectiveness in low-light conditions and makes it the first method capable of tackling three distinct computer vision tasks within a single approach, further highlighting its robustness and adaptability beyond its original scope.

This paper is organized as follows. We provide a brief introduction to the field of color constancy in Sec. 2. We detail the proposed method in Sec. 3. We present our comprehensive experimental discussion in Sec. 4. Lastly, we give a brief summary of the study in Sec. 5.

2 Computational Color Constancy

In the area of color constancy, we generally work with Lambartian surfaces, which reflect light uniformly in all directions. Additionally, we assume that the capturing device consists of three distinct sensors, each of which responds to a different segment of the visible spectrum, which is commonly categorized as short-, middle-, and long-wavelengths. Under these assumptions, the captured image I can be mathematically modeled in terms of the irradiance E falling on the camera sensors, and the spectral sensitivity function S that characterizes the sensor's response to incoming light at a given wavelength:

$$I(x, y) = \int_w E(x, y; \lambda) S_i(\lambda) d\lambda, \tag{1}$$

where (x, y) denotes the spatial coordinates, λ represents the wavelength within the visible spectrum w, and $i \in$ short, middle, long denotes the specific sensor channel.

Since the irradiance E reaching the camera's sensors depends on the reflectance $R(x, y; \lambda)$ of the scene, the light source $L(x, y; \lambda)$, and the scaling factor $G(x, y)$ that represents the scene's geometry, it can be mathematically formulated as:

$$E(x, y; \lambda) = G(x, y) R(x, y; \lambda) L(x, y; \lambda), \tag{2}$$

where the term $G(x, y)$ is typically represented as $\cos \alpha$, with α being the angle between the surface normal and the illumination direction.

Therefore, by using the Eqns. 1 and 2, any image can be mathematically expressed as follows:

$$I(x, y) = G(x, y) \int_w R(x, y; \lambda) L(x, y; \lambda) S_i(\lambda) d\lambda. \tag{3}$$

Generally, in computational color constancy, the main objective is to estimate the color of the illuminant. Despite the simplifications introduced by the Lambertian image formation model, the problem remains under-constrained due to the unknown sensor characteristics of the capturing devices and varying illumination conditions in real-world settings. Therefore, to further relax the challenging nature of the problem, we commonly rely on additional assumptions. For instance, we assume that the scene is illuminated by a uniform light source, the

camera sensors' responses are narrow-band (i.e., approximating Dirac delta functions), and the term G does not significantly impact the estimation of the illuminant (Ebner 2007). Consequently, we can model a color cast image as being uniformly scaled by the light source, and express it as the element-wise product of the (shaded) reflectance and the global illuminant $\mathbf{L}$ as follows:

$$I(x, y) = R(x, y) \cdot \mathbf{L}. \tag{4}$$

Under all of these assumptions, we have a simplified yet effective image formation model for illuminant estimation, forming the basis of many computational color constancy studies. Using traditional methods or machine learning approaches, we can estimate the illuminant $\mathbf{L}$ and eliminate its effect, producing white-balanced images that appear as if they were captured under neutral lighting, thereby allowing more accurate processing of the color features in the scene.

Numerous single-illuminant color constancy algorithms have been introduced to the literature which can be broadly grouped into two categories: traditional methods and learning-based models. Traditional approaches rely on image statistics, with notable examples being the white-patch Retinex and the gray world algorithm (Land 1977; Buchsbaum 1980). The white-patch Retinex method considers the neuroscientific findings indicating that our visual system might be discarding the effects of the illuminant by relying on the highest luminance patch (Land 1977). Therefore, it computes the color vector of the light source by taking the maximum responses of the image channels individually. The gray-world method takes into account that space average color might play a crucial role in our visual system (Buchsbaum 1980). Thus, it computes each image channel's mean separately to estimate the illuminant. As methods inspired by observations of the human visual system tend to prove effective, various algorithms based on these methods, and other findings on our visual system have been proposed to estimate the illuminant (Finlayson and Trezzi 2004; Van De Weijer et al. 2007; Gijsenij et al. 2009; Joze et al. 2012; Cheng et al. 2014; Qian et al. 2018, 2019; Ulucan et al. 2023a,b; Gao et al. 2014, 2015; Zhang et al. 2016; Gao et al. 2019). On the other hand, learning-based models (Afifi and Brown 2019; Laakom et al. 2019; Afifi and Brown 2020a; Afifi et al. 2021, 2022; Domislović et al. 2022; Kim et al. 2025) mainly relying on neural networks have a tendency to achieve higher scores on well-known benchmarks compared to traditional algorithms. Yet, it is reported that in case learning-based models are given scenes with different statistical distributions and/or images taken with capturing devices having unknown specifications they may experience a decline in their performance (Gao et al. 2017; Qian et al. 2019; Ulucan et al. 2022b). As we explicitly demonstrated in our previous study (Ulucan et al. 2022b) and as pointed out in a recent work of Buzzelli et al. (2023), several factors contribute to this drop in performance. First of all, widely used datasets are generally gathered using devices with similar sensor response characteristics. Secondly, the illumination conditions in most benchmarks are quite uniform, e.g., lighting at the edges and/or outside of the color temperature curve is rarely taken into account. Lastly, learning-based methods generally assume that the training and test sets have comparable properties.

As aforementioned, the assumption of a single light source present in the environment can be efficient, yet this assumption frequently fails in practical scenarios due to shadows, multiple light sources, and interreflections (Ershov et al. 2023). On the other hand, multi-illuminant color constancy algorithms, which consider spatially varying illumination, may

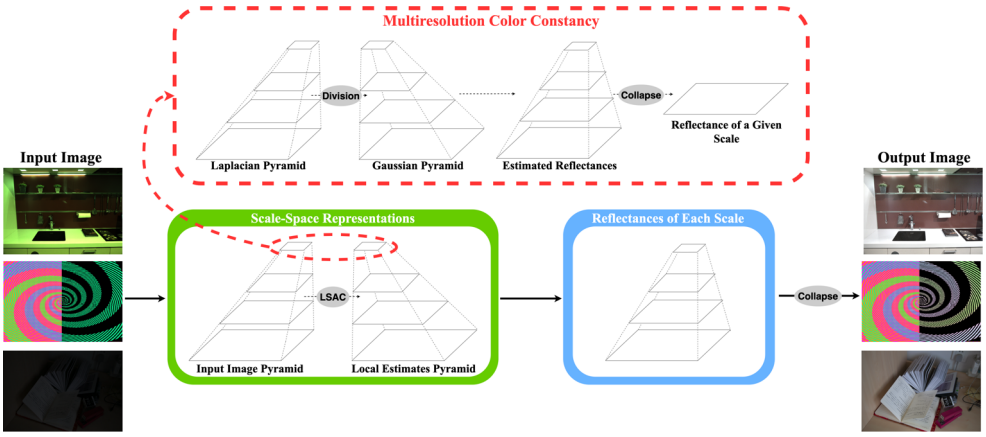

Fig. 2 Flowchart of the proposed method. Our approach simultaneously addresses three different tasks: (i) color constancy, (ii) color assimilation illusions, and (iii) low-light image enhancement through the *multiresolution color constancy* strategy, which performs scale-space within scale-space computations.

address these challenges, however, such methods are considerably rarer compared to those assuming the presence of a single illuminant (Ebner 2009; Bianco et al. 2017; Afifi et al. 2022; Ulucan et al. 2023c).

While most of the aforementioned methods focus on estimating the illuminant from linear images to achieve color constancy, there are also approaches that aim to generate canonical images for sRGB images, without the need to explicitly compute the illuminant or rely on linear images (Afifi et al. 2019; Afifi and Brown 2020b,a; Afifi et al. 2022; Kınlı et al. 2023; Serrano-Lozano et al. 2025). These methods utilize techniques such as nonlinear color mapping, image fusion, and deep neural networks to produce white-balanced images directly from the input scene, without requiring an explicit illuminant estimation step (Serrano-Lozano et al. 2025).

3 Proposed Method

As mentioned in Sec. 1, our method is designed to address two visual phenomena, namely, color constancy and color illusion perception. It is the first computational color constancy study that effectively addresses these computationally opposing phenomena while also demonstrating strong performance in a different computer vision task, i.e., low-light image enhancement (Fig. 2).

The proposed method is based on key observations in human color processing. Studies indicate that the information necessary for illumination estimation is present in the stimulus at the appropriate scale (Shapiro and Lu 2011; Shapiro et al. 2018). Additionally, the effects of the illuminant are primarily captured in the low spatial frequency components, meaning that removing blurry content from images can produce outputs that closely align with human perceptual experience (Shapiro and Lu 2011; Dixon and Shapiro 2017; Shapiro et al. 2018). Furthermore, as demonstrated in Land's experiments (Land 1974), the space average color of the scene plays a critical role in human color processing, particularly in the context of color constancy, a concept further supported by prior studies (Buchsbaum 1980; Linnell and

Foster 1997; Ebner 2007). It is important to emphasize that although we took inspiration from the human visual system, we do not claim that our approach perfectly models it, as its mechanisms are still not fully understood. In short, our goal is not to entirely replicate the operations of the human visual system but to develop a method for computational color constancy that also accounts for color assimilation illusions from the perspective of computer vision.

In this section we first revisit the local space average color algorithm while also explaining our modification, and then we detail our method.

3.1 Revisiting Local Space Average Color

In our method, we use the local space average color algorithm proposed by Ebner (2004) which uses only low-level processing and aligns closely with mechanisms in the human visual system. We consider this algorithm in our method due to various reasons. First of all, studies in behavioral experiments and computational neuroscience suggest that local contrasts between neighboring cones provide key cues for human color constancy (Song and Veltz 2019; Gegenfurtner 2003; Foster and Nascimento 1994). Additionally, research highlights that the average color within a local spatial region plays a crucial role in color perception and color constancy (Linnell and Foster 1997; Gegenfurtner 2003; Ebner 2004). Furthermore, Land's experiments (Land 1974) emphasize the significance of spatial interactions in color perception, and show that color appearance is influenced by surrounding context. In these experiments, Land showed that when individuals focused solely on the center of the colored patches in the Mondrian image, they perceived the patches as grayish-white. However, when observing the Mondrian image as a whole, the observers were able to correctly identify the true reflectance of the patches.

The local space average color method determines the color of light sources through an iterative approach as follows (Ebner 2009):

$$a_i'(x,y) = \frac{1}{\mid N(x,y) \mid} \sum_{(x',y') \in N(x,y)} a_i(x',y') \tag{5}$$

$$a_i(x,y) = I_i(x,y)p + a_i'(x,y)(1-p), \tag{6}$$

where a is the space average color, N represents a group of neighborhood pixels, p adjusts the size of the area where the local space average color is calculated, e.g., a small p value refers to a large area, and subscript i corresponds to the color channels of the image, $i \in \{r,g,b\}$.

This iterative approach is effective, yet it can be computationally expensive due to its convergence time. To reduce the run-time while maintaining similar accuracy, a convolution operation can be applied to compute the space average color as follows:

$$a_i(x,y) = k(x,y) \int \int I_i(x,y) g(x-x', y-y') dx' dy', \tag{7}$$

where i denotes the color channels of the image, $i \in \{r,g,b\}$, and the scaling factor k is determined such that

$$k(x,y) \int \int g(x',y') dx' dy' = 1, \tag{8}$$

where g is the two-dimensional Gaussian kernel given as $\frac{1}{2\pi\sigma^2}exp(-\frac{x^2+y^2}{2\sigma^2})$. σ is the scale of the kernel, which is commonly set as $\sigma = \gamma(\max\{h, w\}/2)$, where h and w are the rows and columns of the image, respectively. Since the local space average color algorithm assumes that the scene's average color is achromatic which is only valid when the scene includes a broad spectrum of colors (Ebner 2009), it is essential to select a σ-value making certain that the local averaging process spans an adequately large area containing a diverse range of objects with different reflectance properties. Therefore, we use a larger σ in scenes with a single light source, and a smaller σ in scenes containing multiple light sources.

Once we obtain the space average color of the scene, we compute the reflectance o of the input as follows:

$$o(x, y) \approx \frac{I(x, y)}{fa(x, y)}, \tag{9}$$

where f represents a uniform scaling factor employed across all color channels and is fixed at 2, assuming that the objects are oriented perpendicularly to the capturing device (Ebner 2009).

To further improve the efficiency of the algorithm, a variant of the method that utilizes depth information while performing local averaging was introduced by Ebner and Hansen (2013). Their main motivation is based on the observation that distinct objects within a scene can lead to significant discontinuities in depth. Hence, regions separated by substantial differences in depth should be handled independently during the estimation of the illuminant. While depth information can enhance the performance of the algorithm, the unavailability of depth maps and potential noise in the range data can reduce the efficiency of the illumination estimation task, thereby limiting the method's usability. Therefore, while we adopt the fundamental principle established in the work of Ebner and Hansen (2013), we prefer to use the gradients of the scene instead of utilizing depth information. We substitute depth with gradients since it is known that significant depth discontinuities cause large gradient changes (Yucer et al. 2016). In order to maintain the consistency of local information and respect edge details, we apply an edge-aware smoothing filter (He et al. 2012) to the local estimates a. Since guided filtering operates under the assumption that the manipulated image locally resembles a linear transformation of the guidance image (He et al. 2012), this additional processing step helps us to maintain gradient variations in the local estimations based on the input image.

3.2 Multiresolution Color Constancy

As discussed in Sec. 1, the proposed method is designed to tackle both computational phenomena, i.e., generating canonical images from color cast scenes while simultaneously mimicking our perception of color assimilation illusions by being deceived by them. Achieving these computationally opposing tasks within a single pipeline is made possible by our novel white-balancing strategy, which uses scale-space within scale-space computations, a technique we term *multiresolution color constancy*.

Such an approach is essential because directly applying Eqn. 9 to scale the pixel intensities of the input scene based on their local estimates would effectively discount the effects of the light source and achieve white-balancing, however, this would come at a cost of failing to replicate our perception of color assimilation illusions within a single framework. For instance, as illustrated in Fig. 3, the multi-illuminant color constancy algorithms GI (Qian et al. 2019) and LSAC (Ebner 2004), despite their ability in producing visually compelling

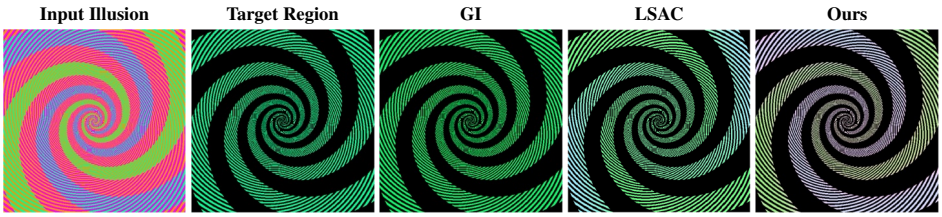

Fig. 3 Brief visual investigation of color assimilation illusions using multi-illuminant color constancy methods and the proposed approach. While white-balancing algorithms focus on mimicking our ability of color constancy, their illumination estimation strategies are insufficient for replicating our perception on illusions. In contrast, the proposed method can address both computationally opposing phenomena.

results for color constancy, struggle to accurately capture the effects of color assimilation illusions, hence fail to mimic our sensation on illusions. In contrast, our proposed strategy successfully handles both color assimilation illusions and color constancy within a single computational framework.

Our method supports both linear RGB and sRGB images. In case of an sRGB image is provided to the algorithm, we perform gamma correction to preserve the linear relationship between the pixel values (Ebner 2007). However, it is important to stress that this step represents an oversimplification, as it neglects the non-linearity introduced by most cameras before obtaining the final sRGB images, as discussed by Afifi et al. (2019).

Following the preprocessing stage, we find the number of pyramid levels, denoted as $n_{\mathcal{L}}$, based on the image resolution, where $n_{\mathcal{L}} = \lfloor \log_2(\min(h, w)) \rfloor - 2$, with h and w representing the height and width of the image. We exclude the two coarsest layers of the image pyramid because locality is negatively affected at these levels. We prefer to adaptively choose the number of scales since images may vary in resolution, and fixed settings could affect the performance negatively. Once the number of scales is determined adaptively, we obtain the representations of the input image at each level. Additionally, for each image representation in the pyramid, we obtain the pixel-wise estimations using the modified version of the local space average color method. One might question why we compute the local space average color at each scale, rather than computing it only at the finest level and then propagating the estimates through the pyramid. While this approach would reduce the complexity of the method, it introduces a significant drawback: it leads to degradation of the local estimates, particularly at coarser scales. As demonstrated in Fig. 4, carrying the estimation from the finest scale to the coarser levels distorts the locality. This issue is less pronounced when pixel-wise estimations are obtained independently at each scale, benefiting both color assimilation illusions and color constancy. For instance, as shown on the first row of Fig. 4, local estimates at the coarsest scale are considerably more distorted when the local space average color is computed only at the finest scale. In contrast, computing the pixel-wise estimates at each scale separately preserves key details, such as the sharp transitions caused by illumination changes, like brighter regions and shadows, which enhances color constancy performance (for more details, see Sec. 4.2.3). Thus, we obtain the pixel-wise estimations of the scene at each pyramid level to maintain as much locality as possible. As demonstrated in Fig. 4, this approach is crucial, particularly for handling color assimilation illusions and multi-illuminant color constancy effectively.

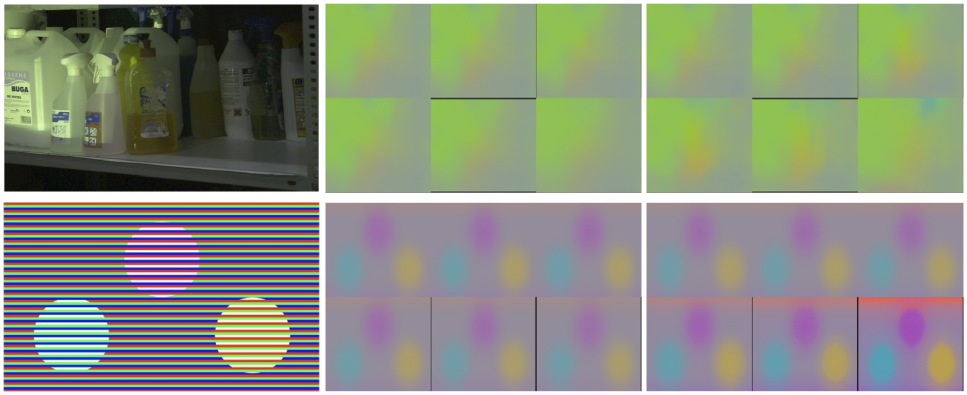

Fig. 4 Illustration of scale-space computations. (Left-to-right) The input image, the estimation computed only at the finest scale and propagated through the pyramid, and the estimations computed independently at each scale. In the estimates, the top-left image shows the finest scale, while the bottom-right image represents the coarsest scale. Computing the estimations at each scale separately preserves details more effectively.

Once the representations of the input scenes and their corresponding local estimates are obtained, we apply our multiresolution color constancy method. Let l represent a pyramid level, where $l \in \{1, ..., n_{\mathcal{L}}\}$. At each level l, we generate a Gaussian pyramid for the local estimates, denoted as $G\{a_l(x, y)\}$, and a Laplacian pyramid for the input scene, denoted as $L\{I_l(x, y)\}$. The number of scales, $\mathcal{S}$, for both pyramids is determined according to the image resolution, as described earlier.

After forming both pyramids, we obtain the (shaded) reflectance at scale s using an operation similar to the one described in Eqn. 9:

$$\mathcal{P}\{o_l(x, y)\}^s = \frac{\mathcal{L}\{I_l(x, y)\}^s}{\mathcal{G}\{a_l(x, y)\}^s}, \quad s = 1, 2, \ldots, \mathcal{S}. \tag{10}$$

This operation is applied across all scales in $\{1, ..., \mathcal{S}\}$ to produce a resulting pyramid $\mathcal{P}\{o_l(x, y)\}$. Afterwards, we collapse this pyramid to obtain an output for the l-th level. This procedure is repeated for each level in $\{1, ..., n_{\mathcal{L}}\}$, which generates a pyramid containing the (shaded) reflectances at all levels. Finally, we collapse this pyramid again to produce a single output (shaded) reflectance o.

As a final stage, we enhance the luminance component of our result. The main motivation for this process is to further mimic the capabilities of the human visual system from the perspective of computer vision. The human visual system adjusts its sensitivity to the surrounding luminance by expanding its response range (Shapiro et al. 2018). This adaptation can be mimicked in computer vision through histogram equalization, as it allows modification of the statistical distribution of an image dimension to maximize the number of distinguishable levels along that dimension (Shapiro et al. 2018). To mimic this aspect of the visual system, we adjust the perceived luminance of the scene by first extracting a *luminance layer* from the input image. To obtain this layer, we first compute the mean value for each color channel and scale the image accordingly, i.e., we apply the gray world assumption (Buchsbaum 1980). Then, we convert the scaled RGB image to CIELAB color space using the $D65$ reference white point (we observed that using alternative white points has a negligible effect

on the results). Then, we perform histogram equalization (Zuiderveld 1994) on the L^* component of the image to enhance its contrast. The resulting L^* component becomes the luminance layer, which we merge with the a^* and b^* color channels of the obtained (shaded) reflectance. After merging these components, the resulting image is transformed back to the RGB color space, which becomes the final output image of the proposed method.

3.3 Application to Low-Light Image Enhancement

Scenes captured under insufficient lighting are referred to as low-light images which mostly contain issues such as lack of sharpness, color distortion, narrow gray range, noise, and lower contrast levels (Wang et al. 2020; Rasheed et al. 2023). The improvement of these images is important for applications such as autonomous navigation, medical diagnostics, and security monitoring (Rasheed et al. 2023).

To tackle the challenges of low-light conditions, both hardware and software solutions have been introduced. While hardware approaches can be costly and require high precision in manufacturing, software methods offer a more flexible and economical alternative (Wang et al. 2020). In recent years, various enhancement techniques relying on learning-based models have been proposed to overcome the challenges of the field (Wei et al. 2018; Chen et al. 2019; Zhang et al. 2019; Wang et al. 2019; Moran et al. 2020; Li et al. 2020; Xu et al. 2020; Kosugi and Yamasaki 2020; Jiang et al. 2021; Liu et al. 2021; Yang et al. 2021; Cai et al. 2023).

To further present the usability of our algorithm beyond its original scope, we investigate its performance in the field of low-light image enhancement. During our experiments we realized that our color constancy algorithm performs well on enhancing low-light images (results are provided in Sec. 4.3.2). However, we observed that simple modifications made without changing the multiresolution color constancy approach can further improve its performance. Particularly, we slightly modified the extraction of the luminance layer by using a percentile-based contrast stretching approach instead of histogram equalization, to improve its performance even further.

In the extraction of the luminance layer, we apply the gray-world algorithm (Buchsbaum 1980) to the input scene. Subsequently, we transform this white-balanced image into the CIELAB color space where we extract the luminance component L^*. Then, we adopt a contrast stretching method based on percentiles to improve the contrast of the extracted luminance component L^*, while reducing the impact of extreme values. First, we determine the 0.5th and 99.5th percentiles of the intensity distribution of L^*. We set values below the 0.5th percentile to the minimum intensity, and values more than the 99.5th percentile to the maximum intensity. We apply these same thresholds to the L^* channel of the output (shaded) reflectance o to obtain a consistent enhancement in contrast. Then, we average the improved L^* channels of the input and the output reflectance. Lastly, we merge the averaged luminance with the a^* and b^* chromaticity channels from the output reflectance, and transform the resulting image into the RGB color space to generate our final output.

4 Experiments and Discussion

We analyze the performance of our method on the different tasks by utilizing various datasets and metrics. In Sec. 4.1, we provide our investigation on color assimilation illusions, while in

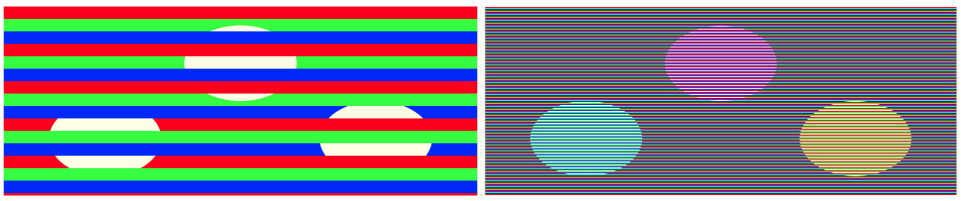

Fig. 5 The perception of a color illusion is strongly influenced by the characteristics of the inducers. As shown in the first column, an image with a low inducer frequency (with thick inducers) hardly evokes an illusion sensation. However, when the frequency of the inducers is increased (the thickness of the inducer is reduced) as demonstrated in the second column, the illusion sensation becomes more apparent.

Sec. 4.2 we present our outcomes on color constancy. Then, in Sec. 4.3, we demonstrate the performance of our method for the task of low-light image enhancement.

4.1 Experiments on Color Illusions

Before starting our discussion on color illusions, we detail our illusions set which we utilize in our experiments, and then we provide our visual results on color assimilation illusions.

4.1.1 Experimental Setup for Color Illusions

The strength of the illusion we perceive depends on the frequency of occurrence of the inducer. As presented in Fig. 5, if we decrease the inducer's frequency of occurrence, the illusion sensation almost vanishes. However, when we increase the frequency of the inducers, we obtain a strong illusion effect. While creating our set, we consider this impact of the inducers, hence we obtain/gather illusions having different frequencies and thicknesses. Moreover, we use a wide range of shapes and colors. Consequently, we create a set that considers images having different shapes, colors, thicknesses and frequencies, which spans a spectrum from those which subtly evoke an illusion effect to those that strongly convey an illusion sensation (Fig. 6).

It is also important to highlight how we analyze our results on the illusions. Studies generally follow two approaches to analyze an algorithm's ability to replicate our sensation. They either visually analyze the target region, the region of interest where we perceive the sensation, or examine intensity changes within the target region. However, neither method provides a statistical investigation, as no error metric or dataset with ground truths exists for color assimilation illusions. This lack of standardized quantitative evaluation remains a key challenge of this field. Yet developing metrics and datasets is also a complex issue, especially when we consider the individual differences of the sensory processing in human color vision, which is highlighted in several studies (Emery and Webster 2019; Shi et al. 2024). Even among the observers with normal vision, the cone sensitivities vary from individual to individual, making it harder to create a dataset or metric for color illusions. Furthermore, even if multiple human subjects perceive a target region as green, the exact shade of the color may differ for each person. Due to these challenges, many studies rely on intensity analysis or visual inspection (Marini and Rizzi 2000; Funt et al. 2004; Corney and Lotto 2007). In this study, we assess our algorithm's performance through visual inspection of the target regions.

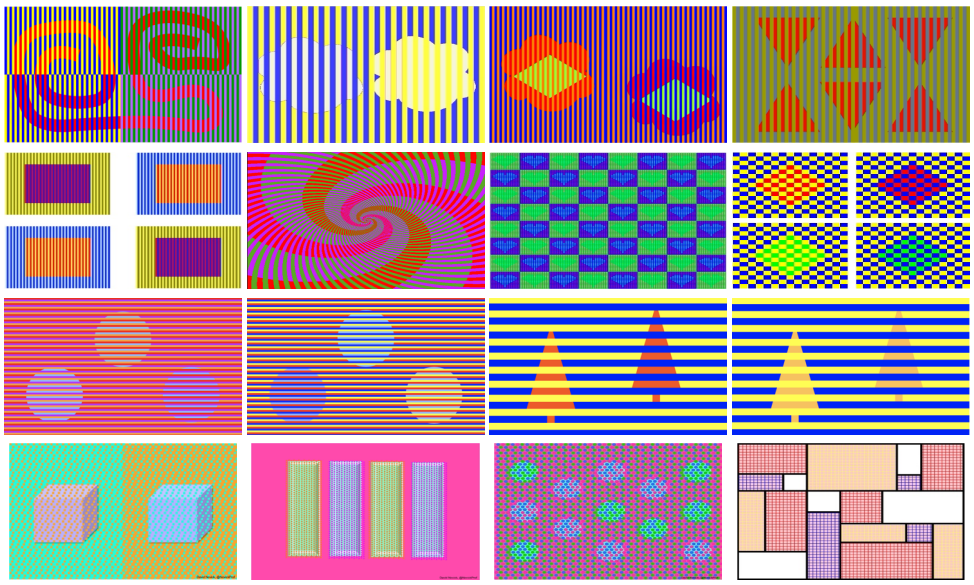

Fig. 6 Example images from our illusion set. The images on the first row are created by ourselves, while the remaining images are courtesy of Akiyoshi Kitaoka, Michael Bach, and David Novick, respectively.

4.1.2 Experimental Results for Color Illusions

We provide our algorithm's results on a variety of color illusions featuring different shapes and color combinations in Fig. 7. We present estimation results at multiple scales and also corresponding target outputs. As demonstrated in Fig. 7, our algorithm is deceived by various color illusions. For instance, in the illusion on the fifth row of Fig. 7, it mimics our perception by providing an output target where the disks are purple and green, while their true reflectance is bluish as presented in the input target. Furthermore, in the illusion at the bottom where we perceive the target region as if it has reversed colors, i.e., blue as green and green as blue, it accurately mimics our sensation.

As seen in the estimates we provide for the different scales, coarser levels exhibiting a stronger illusion effect can be assigned greater importance. This suggests that since the necessary information for accurately estimating the illuminant exists at the appropriate scale within the stimulus (Shapiro and Lu 2011; Shapiro et al. 2018), the same may apply to color illusions, which implies that there is a connection between color assimilation illusions and color constancy. Thus, we should further explore this relationship.

4.2 Experiments on Color Constancy

In this section, first, we present our experimental setup where we provide an overview of widely used color constancy datasets and commonly adopted error metrics. Afterwards, we present our results on 5 different benchmarks that contain scenes with single and multiple illuminants.

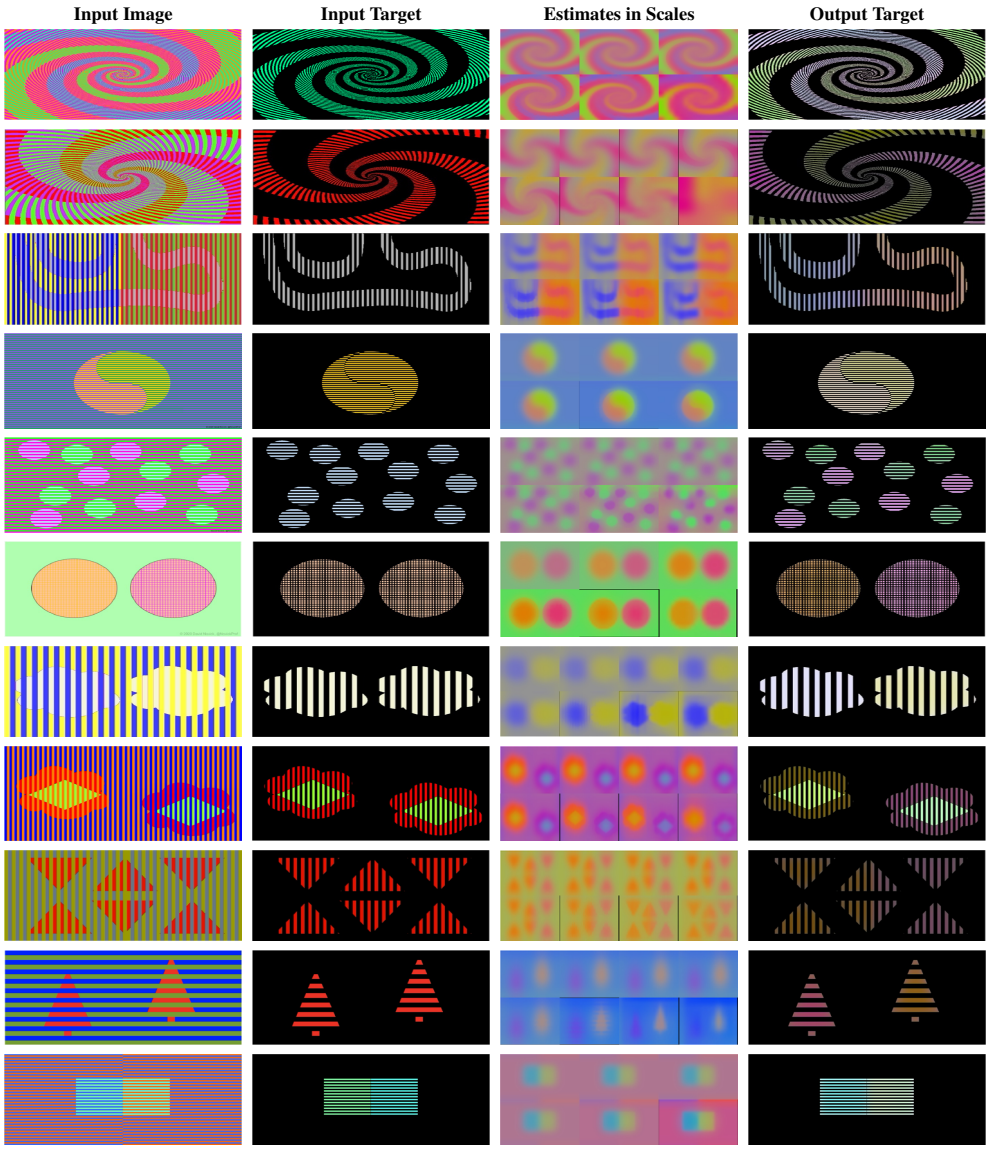

Fig. 7 Visual results of the proposed method applied to color illusions. (Left-to-right) The input image, the target region of the input, the estimations at each scale, and the target area of the proposed method. As our visual system, our algorithm is deceived by various color illusions having different inducer frequencies/thicknesses, colors, and shapes. It is important to note that the colors in the output target may appear darker than in the input image due to the black background in the output target. Also, to accurately assess the color illusions, we would like to emphasize the importance of zooming in and focusing on each image individually. Viewing the image at a small size or from a distance may create a false impression that there is an illusion effect while there is none or only a weak one. Additionally, since peripheral vision is naturally blurred, i.e., locally disordered (Koenderink and van Doorn 2000), even subtle illusions may appear stronger due to color shift of the target area towards that of its surrounding pixels.

4.2.1 Experimental Setup for Color Constancy

We use 5 benchmarks, namely, the Multiple Illuminant and Multiple Object (MIMO) dataset (Beigpour et al. 2013), the Mixed-Illumination Test Set (Afifi et al. 2022), the Rendered WB Dataset (Set 2) (Afifi et al. 2019), the ColorChecker RECommended dataset (Hemrit et al. 2018), and the INTEL-TAU dataset (Laakom et al. 2021) in our evaluations.

The MIMO dataset (Beigpour et al. 2013) includes 78 images across two different sets: the Real-World set and the Laboratory set. While the former contains 20 complex scenes, the latter consists of 58 much simpler scenes. The MIMO dataset provides ground truth pixel-wise illumination maps for each input scene, making it particularly useful for algorithms that output pixel-level illumination estimates rather than just a single vector representing the color of the light source. The Mixed-Illuminant Test Set (Afifi et al. 2022) is rendered by computer graphics, hence, the ground truths are not biased by camera sensor specifications. The synthetic dataset contains a total of 150 images with 30 varying scenes. Each scene is rendered with 5 different mixed illumination conditions at different color temperatures, and for each scene, the ground truth white-balanced image is provided. The Rendered WB Dataset (Set 2) (Afifi et al. 2019) contains over 2,881 images captured from various cameras. For every image exhibiting incorrect white-balance, there is a corresponding correctly white-balanced sRGB image rendered in a standard picture style.

Apart from these datasets we provide results on 2 single-illuminant datasets that were not included in our previous study (Ulucan et al. 2024a). The ColorChecker RECommended dataset (Hemrit et al. 2018) is the updated version of the dataset introduced by Gehler *et al.* (Gehler et al. 2008) which was revised after concerns were raised about the accuracy of the ground truths. It includes a total of 568 scenes. Overall, the dataset consists of 229 close-up shootings, 254 indoor scenes, and 85 outdoor scenes, all taken with two different devices: the Canon 1D and Canon 5D (Buzzelli et al. 2023). Alongside the images, for each scene, the actual color vector of the single light source is also provided. It is important to stress that while this benchmark is widely adopted in many studies, the revised version still contains some minor issues related to illumination conditions. As first pointed out by Cheng et al. (2016) and later by Qian et al. (2019), the benchmark includes 66 images illuminated by two different light sources. The INTEL-TAU dataset (Laakom et al. 2021) is one of the largest benchmarks that contains 7,022 images, including 3,229 close-up images, 1,466 indoor scenes, and 2,327 outdoor scenes (Buzzelli et al. 2023). The INTEL-TAU dataset includes images captured by three different cameras both DSLR and mobile phone devices: the Sony IMX135, Canon 5DSR, and Nikon D810. All the images in this dataset are preprocessed, meaning that their black level is calibrated, they are in linear space, and all sensitive data, such as faces and vehicle license plates, is masked out. On the other hand, this dataset contains several sets with scenes where the calibration object, i.e., a color checkerboard, is unmasked. When evaluating color constancy algorithms, it is crucial to mask out the calibration object from the scene, as these *artificial objects* can bias the performance of the algorithms, thereby preventing a fair evaluation. By removing calibration objects, the algorithms will predict the color vector of the light source based solely on the scene content, rather than relying on artificial or controlled elements that might not be present in real-world scenarios. For this reason, in this study, we only use the images from the "*field1*" and "*field3*", as the calibration object is unmasked in other sets, and the masks indicating the position of the calibration object are not provided.

We would like to highlight that, for the experiments we perform on the ColorChecker RECommended and the INTEL-TAU datasets, in optimal conditions, we need pixel-wise white-balanced ground truths to evaluate our algorithm which relies on local computations. However, both of these benchmarks provide only single RGB vectors for the illuminant as ground truths. Therefore, we use the same RGB vector for each spatial location in the image by noting that shadows, reflections, and sometimes the presence of more than one illuminant in the scenes which is reported in many studies (Cheng et al. 2016; Qian et al. 2019; Ershov et al. 2023) might affect the statistical evaluation of our algorithm.

In order to provide quantitative comparisons by following the common practice, we report the mean and median (Q2) of the angular errors for the MIMO dataset and the mean, median, best-%25 (Q1), and worst-%25 (Q3) of the angular errors for the Rendered Mixed-Illumination Test Set, Rendered WB (Set 2), ColorChecker RECommended, and INTEL-TAU datasets. Alongside the angular error, we also provide the mean, Q1, Q2, and Q3 of the $\triangle$**E**2000 (Sharma et al. 2005) scores for the Rendered Mixed-Illumination Test Set and Rendered WB (Set 2). The learning-based models are highlighted with an asterisk (*) in the tables. We would like to note that *Single-Scale* denotes the version of our method that operates on a single scale, i.e., the version that does not perform multiresolution color constancy, thus does not address color illusions.

Table 1 Statistical results on MIMO dataset. The results are reported based on our recent publication (Ulucan et al. 2024a). The top results are highlighted by using color coding: **best**, **second-best**, third-best best, second-best, and third-best.

	Real-World		Laboratory	
Algorithms	**Mean**	**Q2**	**Mean**	**Q2**
max-RGB (Land and McCann 1971)	6.8°	5.7°	7.8°	7.6°
GW (Buchsbaum 1980)	5.3°	4.3°	3.5°	2.9°
SoG (Finlayson and Trezzi 2004)	6.2°	3.7°	4.9°	4.6°
1^{st} - GE (Van De Weijer et al. 2007)	8.0°	4.7°	4.3°	4.1°
WGE (Gijsenij et al. 2011)	7.9°	4.1°	4.4°	4.0°
GP (Qian et al. 2018)	5.8°	5.0°	13.3°	12.6°
BBCC (Ulucan et al. 2023a)	4.8°	3.6°	3.1°	2.8°
BIO-CC (Ulucan et al. 2022a)	5.0°	4.3°	4.2°	4.1°
Gijsenij *et al.* with maxRGB (Gijsenij et al. 2011)	4.2°	3.8°	5.1°	4.2°
CRF with max-RGB (Beigpour et al. 2013)	4.1°	3.3°	3.0°	2.8°
Akazawa *et al.* with max-RGB (Akazawa et al. 2022)	4.1°	3.4°	2.6°	2.2°
CCATI (Hussain et al. 2019)	3.8°	3.8°	2.6°	2.6°
GI (Qian et al. 2019)	3.9°	3.4°	2.7°	2.2°
C3AE* (Laakom et al. 2019)	12.4°	12.3°	13.9°	14.1°
SIIE* (Afifi and Brown 2019)	5.9°	5.1°	9.0°	9.0°
C5* (Afifi et al. 2021)	11.9°	13.0°	7.0°	7.1°
CNN* (Bianco et al. 2017)	3.3°	3.1°	2.3°	2.2°
GAN* (Das et al. 2021)	3.5°	2.9°	-	-
Single-Scale	4.9°	4.2°	2.7°	2.5°
Proposed	3.2°	2.6°	2.7°	2.3°

4.2.2 Experimental Results for Color Constancy

We present the performance of our method on MIMO dataset in Table 1. Our algorithm presents the best results on the Real-World set, while it performs competitively on the Laboratory set. The scenes in the Real-World set include higher complexity compared to the Laboratory set making it more challenging which is also reflected to the scores of the algorithms (Qian et al. 2019). Most of them have a lower angular error on the Laboratory set. In Fig. 8, we visually compare our method against GI (Qian et al. 2019), and SIEE (Afifi and Brown 2019) on the MIMO dataset. Our algorithm produces fewer artifacts, while specularity, which is a challenging feature for color constancy approaches, may slightly decrease its performance.

In Table 2, we provide the scores on the Mixed-Illumination Test Set, and the Rendered WB (Set 2). On both benchmarks, our simple yet effective method presents competitive results compared to the state-of-the-art models. The visual results of our method given in Fig. 9 also demonstrate that our algorithm is effectively able to overcome challenges such as strong illumination conditions.

Additionally, in Table 3, we present our statistical results on the ColorChecker RECommended, and INTEL-TAU datasets, where the scenes are illuminated uniformly. Despite the suboptimal experimental setting caused by the absence of pixel-wise ground truth information, our method outperforms most of the state-of-the-art models. It achieves the third-best result on average for both datasets. Furthermore, it outputs a considerably low angular error for the worst cases (Q3) which is a valuable outcome since in the field of color constancy it is desired to improve the error for these cases (Ulucan et al. 2023c).

As a result, all of the experimental results show that our method can achieve consistent performance across diverse benchmarks and under complex illumination conditions. Furthermore, the statistical results demonstrate that our algorithm, which simultaneously addresses both color constancy and color assimilation illusions, outperforms its single-scale version that cannot reproduce illusions. This provides empirical evidence supporting our claim that the ability to reproduce our sensation on color assimilation illusions is closely linked to improved color constancy performance, thereby highlighting the relationship between the two phenomena from the perspective of computer vision. The experiments also present the fact that by developing simple yet effective algorithms that do not rely on any learning strategy, it is possible to achieve state-of-the-art performance.

Fig. 8 Visual comparison of the proposed method with existing color constancy approaches on the MIMO Real-World dataset. (Left to right): input scenes, results of GI, results of SIEE, and results of our method.

Table 2 Statistical results on Rendered Mixed-Illumination and Rendered WB (Set 2). The results are reported based on our recent publication (Ulucan et al. 2024a). The top results are highlighted by using color coding: best, second-best, and third-best.

	Angular Error				△E 2000			
Mixed-Illumination Test Set	**Mean**	**Q1**	**Q2**	**Q3**	**Mean**	**Q1**	**Q2**	**Q3**
GP (Qian et al. 2018)	19.7°	11.9°	17.2°	27.1°	25.1	19.1	22.6	27.5
GI (Qian et al. 2019)	6.4°	4.7°	5.7°	7.1°	12.8	9.6	12.5	14.6
KNN WB* (Afifi et al. 2019)	5.8°	4.3°	5.8°	6.9°	12.0	9.4	11.6	13.6
Interactive WB* (Afifi and Brown 2020b)	5.9°	4.6°	5.6°	6.6°	11.4	8.9	10.9	12.8
Deep WB* (Afifi and Brown 2020a)	4.5°	3.6°	4.2°	5.2°	10.9	8.6	9.8	12.0
Mixed WB* (Afifi et al. 2022)	5.4°	4.3°	4.9°	6.2°	10.6	9.4	10.7	11.8
Style WB* (Kınlı et al. 2023)	5.7°	4.5°	5.4°	6.3°	12.1	10.4	12.1	13.4
FDM WB* (Kınlı et al. 2025)	5.9°	4.6°	5.9°	6.9°	10.2	8.8	9.8	11.7
Single-Scale	4.8°	3.3°	4.6°	8.1°	11.0	8.1	10.4	14.7
Proposed	4.8°	3.4°	4.4°	6.3°	8.9	6.7	8.5	12.0

	Angular Error				△E 2000			
Rendered WB (Set 2)	**Mean**	**Q1**	**Q2**	**Q3**	**Mean**	**Q1**	**Q2**	**Q3**
max-RGB (Land and McCann 1971)	13.2°	8.2°	12.6°	18.1°	12.9	9.0	13.4	17.1
GW (Buchsbaum 1980)	8.6°	5.4°	7.9°	10.9°	10.7	7.7	10.1	13.2
SoG (Finlayson and Trezzi 2004)	9.0°	5.3°	8.3°	12.0°	9.8	6.9	9.7	12.5
1^{st} - GE (Van De Weijer et al. 2007)	12.5°	7.6°	11.9°	17.0°	13.0	9.1	12.9	16.6
WGE (Gijsenij et al. 2011)	13.5°	7.8°	12.6°	18.6°	14.0	9.0	13.7	18.6
FC4* (Hu et al. 2017)	10.4°	5.3°	9.3°	14.2°	10.8	7.4	10.6	13.8
Quasi-U CC* (Bianco and Cusano 2019)	10.5°	5.9°	9.4°	14.0°	10.7	7.0	10.5	13.9
WB-sRGB* (Afifi et al. 2019)	4.5°	2.3°	3.6°	6.0°	5.6	3.4	4.9	7.1
Single-Scale	8.7°	4.3°	8.0°	14.2°	10.6	6.6	10.3	15.2
Proposed	7.8°	3.7°	7.1°	12.9°	10.3	6.1	10.0	15.2

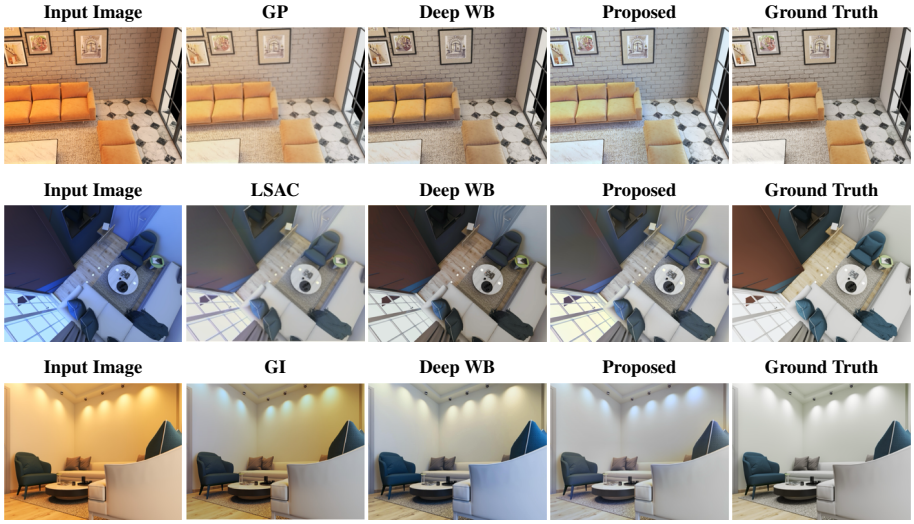

Fig. 9 Visual comparison of the proposed method against both traditional and learning-based methods on indoor scenes.

Table 3 Statistical results on ColorChecker RECommended and INTEL-TAU datasets. The results are reported based on our recent publication (Ulucan et al. 2024c). The top results are highlighted by using color coding: best, second-best, and third-best.

	ColorChecker RECommended				INTEL-TAU			
Algorithms	**Mean**	**Q1**	**Q2**	**Q3**	**Mean**	**Q1**	**Q2**	**Q3**
max-RGB (Land and McCann 1971)	7.78°	1.49°	5.43°	17.47°	10.49°	1.70°	11.14°	19.24°
GW (Buchsbaum 1980)	4.71°	0.93°	3.54°	10.44°	4.90°	0.93°	3.85°	10.59°
1^{st} - GE (Van De Weijer et al. 2007)	5.79°	0.93°	3.68°	14.17°	5.89°	0.94°	4.07°	13.79°
wGE (Gijsenij et al. 2011)	6.08°	0.78°	3.33°	15.57°	5.99°	0.80°	3.63°	14.89°
DOCC (Gao et al. 2015)	7.23°	0.79°	4.26°	18.04°	7.18°	0.80°	4.66°	16.97°
GP (Qian et al. 2018)	3.81°	0.76°	2.96°	8.35°	3.57°	0.64°	2.56°	8.23°
GI (Qian et al. 2019)	3.19°	0.44°	1.90°	8.02°	3.32°	0.56°	2.18°	8.03°
BIO-CC (Ulucan et al. 2022a)	4.40°	0.86°	3.30°	9.84°	4.14°	0.76°	3.05°	9.42°
BBCC (Ulucan et al. 2023a)	3.48°	1.06°	2.71°	7.37°	3.37°	0.79°	2.63°	7.25°
MSCC (Ulucan et al. 2023c)	3.16°	0.62°	2.16°	7.32°	3.23°	0.59°	2.23°	7.47°
BoCF CC* (Laakom et al. 2020)	-	-	-	-	2.90°	0.90°	2.40°	6.10°
Quasi-U CC* (Bianco and Cusano 2019)	3.46°	-	2.23°	-	3.12°	0.60°	2.19°	7.28°
SIIE* (Afifi and Brown 2019)	2.77°	0.55°	1.93°	6.53°	3.42°	0.73°	2.42°	7.80°
C3AE* (Laakom et al. 2019)	2.10°	0.80°	1.90°	4.00°	3.40°	0.90°	2.70°	7.00°
One-Net CCC* (Domislović et al. 2022)	-	-	-	-	3.30°	1.10°	3.20°	5.90°
FFCC* (Barron and Tsai 2017)	2.95°	0.57°	2.19°	6.75°	3.42°	0.70°	2.38°	7.96°
FC4* (Hu et al. 2017)	1.77°	0.34°	1.11°	4.29°	2.60°	0.70°	2.00°	5.50°
C5* (Afifi et al. 2021)	2.50°	0.53°	1.99°	5.46°	2.52°	0.52°	1.70°	5.96°
CNN* (Bianco et al. 2015)	3.23°	0.92°	2.64°	6.54°	3.20°	0.92°	2.56°	6.55°
Revisiting CNNs* (Ulucan et al. 2024c)	2.70°	0.62°	2.00°	5.98°	2.90°	0.79°	2.27°	6.11°
Single-Scale	2.49°	0.91°	2.03°	4.80°	3.45°	1.17°	2.97°	6.55°
Proposed	2.32°	0.68°	1.76°	4.85°	2.67°	0.73°	2.09°	5.59°

4.2.3 Ablation Study

To validate our design choice for our method, we conducted an ablation experiment on subsets of the Gehler and INTEL-TAU datasets. We compared single-scale estimation, propagating estimates from the finest level through the pyramid, and our proposed independent estimation at each scale. As presented in Table 4, the results confirm that propagating estimates leads to significant degradation in accuracy, while the proposed algorithm achieves the best performance. The reason behind this performance difference can be explained by the fact that propagating estimates causes degradation in local coherence which decreases the accuracy of the estimates as also previously discussed in Sec. 3.2 and shown in Fig. 4. These findings support the necessity of computing estimates independently at each scale, as adopted in our method.

Additionally, this ablation study provides insight into the link between color constancy accuracy and illusion reproduction from the perspective of computer vision. The single-scale version cannot reproduce color assimilation illusions, while the proposed method both achieves high color constancy accuracy and addresses illusions.

Table 4 Ablation study comparing single-scale computations, propagation of estimates from the finest level, and the proposed method on subsets of the Gehler and INTEL-TAU datasets. The best results are highlighted in bold.

	ColorChecker RECommended				INTEL-TAU			
Algorithms	**Mean**	**Q1**	**Q2**	**Q3**	**Mean**	**Q1**	**Q2**	**Q3**
Single-scale	2.65°	1.05°	2.18°	4.92°	3.40°	1.28°	2.87°	6.43°
Propagation	4.92°	2.64°	4.21°	8.18°	4.03°	1.86°	3.56°	7.03°
Proposed	**2.28°**	**0.76°**	**1.73°**	**4.68°**	**3.18°**	**1.14°**	**2.71°**	**6.04°**

4.3 Experiments on Low-Light Image Enhancement

In this section, we present a brief investigation on low-light image enhancement. First, we explain our experimental setup and then discuss our results.

4.3.1 Experimental Setup for Low-Light Image Enhancement

We compare our learning-free method against 22 learning-based models, and our initial version (Ulucan et al. 2024a) on 2 widely used benchmarks, namely, the LOL-v1 and LOL-v2 datasets (Wei et al. 2018; Yang et al. 2021). In order to provide a statistical analysis, we use the peak signal-to-noise ratio (PSNR) and the structural similarity index (SSIM) (Wang et al. 2004). Higher PSNR and SSIM scores represent better results. We give quantitative results based on recent comprehensive works (Hou et al. 2024; Cai et al. 2023; Jiang et al. 2025).

4.3.2 Experimental Results for Low-Light Image Enhancement

Quantitative results of our experiments are shown in Table 5. Our algorithm, which is specifically designed for color illusion perception and color constancy, presents competitive results compared to the learning-based models developed for the task of low-light image enhancement. Statistically, it is the third-best algorithm on average.

When low-light scenes exhibit color tints due to illumination effects, many existing methods tend to generate output images with an unwanted color cast, as seen in the first row of Fig. 10. On the other hand, our multiresolution color constancy approach greatly avoids these artifacts. Additionally, in Fig. 10, we can observe that due to the nature of our method it performs both low-light image enhancement and color constancy. Therefore, if the ground truth images include color shifts that our method eliminates, this may affect the quantitative results negatively, although our algorithm effectively improves the scenes. We avoid white-balancing the ground truths to maintain fairness since other low-light image enhancement techniques are evaluated by using the original ground truths.

Lastly, we would like to briefly discuss the advantages and the limitations of our method for its application to low-light image enhancement. One of the important advantages of our algorithm is that it does not require any optimization or extensive parameter tuning. This is beneficial when we would like to avoid the computational cost of the training stages of learning-based models. Moreover, our method operates on a single image, in contrast to fusion-based techniques that need multiple exposure settings. Also, it simultaneously enhances low-light conditions and corrects color casts. On the other hand, in some scenes

Table 5 Statistical comparison of the proposed method against the learning-based low-light image enhancement models, and its initial version (Ulucan et al. 2024a). The top results are highlighted by using color coding: best, second-best, and third-best.

	LOL-v1		LOL-v2			LOL-v1		LOL-v2	
	PSNR	SSIM	PSNR	SSIM		PSNR	SSIM	PSNR	SSIM
Fei et al. (2023)	15.90	0.54	-	-	Wang et al. (2019)	14.38	0.44	13.27	0.45
Moran et al. (2020)	15.28	0.47	14.10	0.48	Fu et al. (2023)	19.51	0.73	-	-
Yang et al. (2023)	19.74	0.74	-	-	Chen et al. (2021)	16.27	0.50	19.80	0.81
Liu et al. (2021)	18.23	0.72	18.37	0.72	Li et al. (2020)	21.46	0.80	17.80	0.79
Ma et al. (2022)	14.78	0.65	20.28	0.75	Xu et al. (2020)	18.27	0.66	16.85	0.67
Yang et al. (2020)	19.86	0.83	20.13	0.83	Jiang et al. (2025)	20.45	0.80	-	-
Wei et al. (2018)	16.77	0.56	15.47	0.56	Kosugi and Yamasaki (2020)	15.23	0.45	14.05	0.45
Yang et al. (2021)	17.20	0.64	20.06	0.81	Jiang et al. (2021)	17.48	0.65	18.23	0.61
Wei et al. (2024)	-	-	20.79	0.79	Nguyen et al. (2024)	23.97	0.84	-	-
Chen et al. (2019)	14.35	0.43	13.24	0.44	Cai et al. (2023)	25.16	0.84	22.80	0.84
Wu et al. (2022)	21.33	0.84	21.16	0.84	Ulucan et al. (2024a)	20.46	0.72	19.66	0.70
Zhang et al. (2019)	20.87	0.80	14.47	0.64	**Proposed**	22.28	0.80	21.58	0.81

Fig. 10 Visual comparison of our method against learning-based models on low-light image enhancement.

our method may be more prone to noise as other traditional methods in this field than the state-of-the-art networks-based strategies. Yet, with this application, we demonstrate that with explainable operations that are built upon the observations on our visual system, our method cannot only address color constancy and color illusions but also perform low-light image enhancement with a competitive performance. This makes our method the first approach in the literature that can perform these 3 different tasks simultaneously with a single pipeline.

5 Conclusion

Our visual system is generally able to identify the true reflectance of objects regardless of the environmental context, yet it sometimes fails to accurately determine the actual colors present in a scene. Color illusions demonstrate how contextual information can fool our perception. Both color constancy and color illusion perception are two phenomena widely studied in the field of computational neuroscience. Nevertheless, it is still unclear how color constancy is achieved or why our perception can be deceived by illusions. However, we do know that there is a link between illusions and color constancy, and an ideal algorithm mimicking our visual system should be capable of replicating both our perception of color illusions and our ability to achieve color constancy. By taking motivation from these observations, we designed a single algorithm that can mimic our behavior on both phenomena. We accomplished this by leveraging observations from various computational neuroscience and computer vision studies, and we introduced our multiresolution color constancy method. Our algorithm relies on scale-space within scale-space operations, and the modified version of the local space average color method. The proposed strategy allows us to estimate the illuminant at each level, and enables us to mimic our sensation on illusions by utilizing information from the coarser scales where the effect of illusions is greater than the finer scales. Furthermore, our method is also able to perform low-light image enhancement by also white-balancing the poorly illuminated images which is an advantage for this task since it eliminates the need of a separate color constancy operation.

To the best of our knowledge, this is the first study introducing a single algorithm that can perform these three distinct computer vision tasks. As future work, we will analyze color illusions by using learning-based strategies, and we will focus on creating evaluation techniques for color illusions.

Acknowledgment

Science would never advance without the kindness and collaboration of others. We would like to express our sincere gratitude to Michael Bach, Akiyoshi Kitaoka, and David Novick for graciously granting us permission to use their color illusions. Their contributions have greatly enhanced our work.

Data Availability

The datasets related to color constancy, and low-light image enhancement are publicly available. The color assimilation illusions which are created by ourselves are available upon request. The remaining illusions are courtesy of Michael Bach, Akiyoshi Kitaoka, and David Novick.

Declarations

The authors have no relevant financial or non-financial interests to disclose.

References

Afifi, M., Brown, M.S.: Sensor-independent illumination estimation for DNN models. In: Brit. Mach. Vis. Conf. (2019). BMVA Press

Afifi, M., Brown, M.S.: Deep white-balance editing. In: IEEE/CVF Conf. Comput. Vis. Pattern Recog., pp. 1397–1406 (2020)

Afifi, M., Brown, M.S.: Interactive white balancing for camera-rendered images. In: Color Imag. Conf., vol. 28, pp. 136–141 (2020). Soc. Imag. Sci. Technol.

Afifi, M., Brubaker, M.A., Brown, M.S.: Auto white-balance correction for mixed-illuminant scenes. In: IEEE/CVF Winter Conf. Appl. Comput. Vis., pp. 1210–1219 (2022)

Afifi, M., Barron, J.T., LeGendre, C., Tsai, Y.-T., Bleibel, F.: Cross-camera convolutional color constancy. In: IEEE/CVF Int. Conf. Comput. Vis., pp. 1981–1990 (2021)

Akazawa, T., Kinoshita, Y., Shiota, S., Kiya, H.: N-white balancing: White balancing for multiple illuminants including non-uniform illumination. IEEE Access **10**, 89051–89062 (2022)

Afifi, M., Price, B., Cohen, S., Brown, M.S.: When color constancy goes wrong: Correcting improperly white-balanced images. In: IEEE/CVF Conf. Comput. Vis. Pattern Recog., pp. 1535–1544 (2019)

Bach, M.: Color Assimilation Illusions. michaelbach.de/ot (Last accessed: 01.04.2025)

Bianco, S., Cusano, C.: Quasi-unsupervised color constancy. In: IEEE/CVF Conf. Comput. Vis. Pattern Recog., pp. 12212–12221 (2019)

Bianco, S., Cusano, C., Schettini, R.: Color constancy using CNNs. In: IEEE Conf. Comput. Vis. Pattern Recog. Workshops, pp. 81–89 (2015)

Bianco, S., Cusano, C., Schettini, R.: Single and multiple illuminant estimation using convolutional neural networks. IEEE Trans. Image Process. **26**(9), 4347–4362 (2017)

Blakeslee, B., McCourt, M.E.: A unified theory of brightness contrast and assimilation incorporating oriented multiscale spatial filtering and contrast normalization. Vis. Res. **44**(21), 2483–2503 (2004)

Brainard, D.H., Radonjic, A.: Color constancy. Vis. Neurosciences **1**, 948–961 (2004)

Beigpour, S., Riess, C., Van De Weijer, J., Angelopoulou, E.: Multi-illuminant estimation with conditional random fields. IEEE Trans. Image Process. **23**, 83–96 (2013)

Barron, J.T., Tsai, Y.-T.: Fast fourier color constancy. In: IEEE/CVF Conf. Comput. Vis. Pattern Recognit., pp. 886–894 (2017)

Buchsbaum, G.: A spatial processor model for object colour perception. J. Franklin Inst. **310**, 1–26 (1980)

Buzzelli, M., Zini, S., Bianco, S., Ciocca, G., Schettini, R., Tchobanou, M.K.: Analysis of biases in automatic white balance datasets and methods. Color Res. Appl. **48**(1), 40–62 (2023)

Cheng, D., Abdelhamed, A., Price, B., Cohen, S., Brown, M.S.: Two illuminant estimation and user correction preference. In: IEEE/CVF Conf. Comput. Vis. Pattern Recog., pp. 469–477 (2016)

Cai, Y., Bian, H., Lin, J., Wang, H., Timofte, R., Zhang, Y.: Retinexformer: One-stage retinex-based transformer for low-light image enhancement. In: IEEE/CVF Int. Conf. Comput. Vis., pp. 12504–12513 (2023)

Chen, C., Chen, Q., Do, M.N., Koltun, V.: Seeing motion in the dark. In: IEEE/CVF Int. Conf. Comput. Vis., pp. 3185–3194 (2019)

Corney, D., Lotto, R.B.: What are lightness illusions and why do we see them? PLoS Comput. Biol. **3**(9), 180 (2007)

Cheng, D., Prasad, D.K., Brown, M.S.: Illuminant estimation for color constancy: Why spatial-domain methods work and the role of the color distribution. J. Opt. Soc. America A **31**, 1049–1058 (2014)

Chen, H., Wang, Y., Guo, T., Xu, C., Deng, Y., Liu, Z., Ma, S., Xu, C., Xu, C., Gao, W.: Pre-trained image processing transformer. In: IEEE/CVF Conf. Comput. Vis. Pattern Recognit., pp. 12299–12310 (2021)

Das, P., Liu, Y., Karaoglu, S., Gevers, T.: Generative models for multi-illumination color constancy. In: IEEE/CVF Conf. Comput. Vis. Pattern Recog., pp. 1194–1203 (2021)

Dixon, E.L., Shapiro, A.G.: Spatial filtering, color constancy, and the color-changing dress. J. Vis. **17**(3), 7–7 (2017)

Domislović, I., Vršnak, D., Subašić, M., Lončarić, S.: One-net: Convolutional color constancy simplified. Pattern Recognit. Letters **159**, 31–37 (2022)

Ebner, M.: A parallel algorithm for color constancy. J. Parallel Distrib. Comput. **64**, 79–88 (2004)

Ebner, M.: Color Constancy, 1st Ed. Wiley Publishing, ISBN: 0470058299, Hoboken, NJ, USA (2007)

Ebner, M.: Color constancy based on local space average color. Mach. Vis. Appl. **20**(5), 283–301 (2009)

Ebner, M., Hansen, J.: Depth map color constancy. Bio-Algorithms and Med-Syst. **9**(4), 167–177 (2013)

Ershov, E., Tesalin, V., Ermakov, I., Brown, M.S.: Physically-plausible illumination distribution estimation. In: IEEE/CVF Int. Conf. Comput. Vis., pp. 12928–12936 (2023)

Emery, K.J., Webster, M.A.: Individual differences and their implications for color perception. Current Opinion Behavioral Sciences **30**, 28–33 (2019)

Funt, B.V., Ciurea, F., McCann, J.J.: Retinex in matlab™. J. Electron. Imag. **13**(1) (2004)

Foster, D.H., Nascimento, S.M.: Relational colour constancy from invariant cone-excitation ratios. Proc. Royal Soc. London. Ser. B: Biol. Sciences **257**(1349), 115–121 (1994)

Fei, Z. B.and Lyu, Pan, L., Zhang, J., Yang, W., Luo, T., Zhang, B., Dai, B.: Generative diffusion prior for unified image restoration and enhancement. In: IEEE/CVF Conf. Comput. Vis. Pattern Recognit., pp. 9935–9946 (2023)

Finlayson, G.D., Trezzi, E.: Shades of gray and colour constancy. In: Color and Imag. Conf., pp. 37–41 (2004). Society for Imaging Science and Technology

Fu, Z., Yang, Y., Tu, X., Huang, Y., Ding, X., Ma, K.-K.: Learning a simple low-light image enhancer from paired low-light instances. In: IEEE/CVF Conf. Comput. Vis. Pattern Recognit., pp. 22252–22261 (2023)

Gegenfurtner, K.R.: Reflections on colour constancy. Nature **402**(6764), 855–856 (1999)

Gegenfurtner, K.R.: Cortical mechanisms of colour vision. Nature Reviews Neuroscience **4**(7), 563–572 (2003)

Gijsenij, A., Gevers, T., Van De Weijer, J.: Physics-based edge evaluation for improved color constancy. In: IEEE Conf. Comput. Vis. Pattern Recog., pp. 581–588 (2009)

Gijsenij, A., Gevers, T., Van De Weijer, J.: Improving color constancy by photometric edge weighting. IEEE Trans. Pattern Anal. Mach. Intell. **34**, 918–929 (2011)

Gao, S., Han, W., Yang, K., Li, C., Li, Y.: Efficient color constancy with local surface reflectance statistics. In: Eur. Conf. Comput. Vis., pp. 158–173 (2014). Springer

Gijsenij, A., Lu, R., Gevers, T.: Color constancy for multiple light sources. IEEE Trans. Image Process. **21**(2), 697–707 (2011)

Gehler, P.V., Rother, C., Blake, A., Minka, T., Sharp, T.: Bayesian color constancy revisited. In: IEEE Conf. Comput. Vis. Pattern Recog., pp. 1–8 (2008)

Gao, S.-B., Ren, Y.-Z., Zhang, M., Li, Y.-J.: Combining bottom-up and top-down visual mechanisms for color constancy under varying illumination. IEEE Trans. Image Process. **28**(9), 4387–4400 (2019)

Gomez-Villa, A., Martin, A., Vazquez-Corral, J., Bertalmío, M.: Convolutional neural networks can be deceived by visual illusions. In: IEEE/CVF Conf. Comput. Vis. Pattern Recog., pp. 12309–12317 (2019)

Gomez-Villa, A., Martín, A., Vazquez-Corral, J., Bertalmío, J. M.and Malo: On the synthesis of visual illusions using deep generative models. J. Vis. **22**(8), 2–2 (2022)

Gomez-Villa, A., Wang, K., Parraga, C.A., Twardowski, B., Malo, J., Vazquez-Corral, J., Weijer, J.: The art of deception: Color visual illusions and diffusion models. In: IEEE/CVF Conf. Comput. Vis. Pattern Recog., pp. 18642–18652 (2025)

Gao, S.-B., Yang, K.-F., Li, C.-Y., Li, Y.-J.: Color constancy using double-opponency. IEEE Trans. Pattern Anal. Mach. Intell. **37**(10), 1973–1985 (2015)

Gao, S., Zhang, M., Li, C., Li, Y.: Improving color constancy by discounting the variation of camera spectral sensitivity. J. Opt. Soc. America A **34**, 1448–1462 (2017)

Hussain, M.A., Akbari, A.S., Halpin, E.A.: Color constancy for uniform and non-uniform illuminant using image texture. IEEE Access **7**, 72964–72978 (2019)

Hemrit, G., Finlayson, G.D., Gijsenij, A., Gehler, P., Bianco, S., Funt, B., Drew, M., Shi, L.: Rehabilitating the colorchecker dataset for illuminant estimation. In: Color Imag. Conf., pp. 350–353 (2018). Society for Imaging Science and Technology

He, K., Sun, J., Tang, X.: Guided image filtering. IEEE Trans. Pattern Anal. Mach. Intell. **35**(6), 1397–1409 (2012)

Hirsch, E., Tal, A.: Color visual illusions: A statistics-based computational model. Advances Neural Inf. Process. Syst. **33**, 9447–9458 (2020)

Hurlbert, A.: Colour constancy. Current Biology **17**(21), 906–907 (2007)

Hu, Y., Wang, B., Lin, S.: Fc4: Fully convolutional color constancy with confidence-weighted pooling. In: IEEE/CVF Conf. Comput. Vis. Pattern Recog. (2017)

Hou, J., Zhu, Z., Hou, J., Liu, H., Zeng, H., Yuan, H.: Global structure-aware diffusion process for low-light image enhancement. Advances Neural Inf. Process. Syst. **36** (2024)

Joze, H.R.V., Drew, M.S., Finlayson, G.D., Rey, P.A.T.: The role of bright pixels in illumination estimation. In: Color Imag. Conf., pp. 41–46 (2012). Society for Imaging Science and Technology

Jiang, Y., Gong, X., Liu, D., Cheng, Y., Fang, C., Shen, X., Yang, J., Zhou, P., Wang, Z.: Enlightengan: Deep light enhancement without paired supervision. IEEE Trans. Image Process. **30**, 2340–2349 (2021)

Jiang, H., Luo, A., Liu, X., Han, S., Liu, S.: Lightendiffusion: Unsupervised low-light image

enhancement with latent-retinex diffusion models. In: Eur. Conf. Comput. Vis., pp. 161–179 (2025). Springer

Kim, D., Afifi, M., Kim, D., Brown, M.S., Kim, S.J.: Ccmnet: Leveraging calibrated color correction matrices for cross-camera color constancy. arXiv preprint arXiv:2504.07959 (2025)

Kubota, Y., Hiyama, A., Inami, M.: A machine learning model perceiving brightness optical illusions: Quantitative evaluation with psychophysical data. In: Proc. Augmented Humans Int. Conf., pp. 174–182 (2021)

Kınlı, F., Özcan, B., Kıraç, F.: Advancing white balance correction through deep feature statistics and feature distribution matching. J. Vis. Communication Image Representation **108**, 104412 (2025)

Koenderink, J.J., Doorn, A.J.: Blur and disorder. J. Vis. Communication Image Representation **11**(2), 237–244 (2000)

Kosugi, S., Yamasaki, T.: Unpaired image enhancement featuring reinforcement-learning-controlled image editing software. In: AAAI Conf Artif. Intell., pp. 11296–11303 (2020)

Kınlı, F., Yılmaz, D., Özcan, B., Kıraç, F.: Modeling the lighting in scenes as style for auto white-balance correction. In: IEEE/CVF Winter Conf. Appl. Comput. Vis., pp. 4903–4913 (2023)

Land, E.H.: The retinex theory of colour vision. Proc. Roy. Institution Gr. Britain **47**, 23–58 (1974)

Land, E.H.: The retinex theory of color vision. Scientific Amer. **237**, 108–129 (1977)

Linnell, K.J., Foster, D.H.: Space-average scene colour used to extract illuminant information. John Dalton's Colour Vis. Legacy, 501–509 (1997)

Li, J., Li, J., Fang, F., Li, F., Zhang, G.: Luminance-aware pyramid network for low-light image enhancement. IEEE Trans. Multimedia **23**, 3153–3165 (2020)

Land, E.H., McCann, J.J.: Lightness and retinex theory. J. Opt. Soc. America A **61**(1), 1–11 (1971)

Liu, R., Ma, L., Zhang, J., Fan, X., Luo, Z.: Retinex-inspired unrolling with cooperative prior architecture search for low-light image enhancement. In: IEEE/CVF Conf. Comput. Vis. Pattern Recognit., pp. 10561–10570 (2021)

Laakom, F., Passalis, N., Raitoharju, J., Nikkanen, J., Tefas, A., Iosifidis, A., Gabbouj, M.: Bag of color features for color constancy. IEEE Trans. Image Process. **29**, 7722–7734 (2020)

Laakom, F., Raitoharju, J., Iosifidis, A., Nikkanen, J., Gabbouj, M.: Color constancy

convolutional autoencoder. In: Symp. Ser. Comput. Intell., pp. 1085–1090 (2019). IEEE

Laakom, F., Raitoharju, J., Nikkanen, J., Iosifidis, A., Gabbouj, M.: Intel-tau: A color constancy dataset. IEEE Access **9**, 39560–39567 (2021)

Mitra, S., Mazumdar, D., Ghosh, K., Bhaumik, K.: An adaptive scale gaussian filter to explain white's illusion from the viewpoint of lightness assimilation for a large range of variation in spatial frequency of the grating and aspect ratio of the targets. PeerJ **6**, 5626 (2018)

Ma, L., Ma, T., Liu, R., Fan, X., Luo, Z.: Toward fast, flexible, and robust low-light image enhancement. In: IEEE/CVF Conf. Comput. Vis. Pattern Recognit., pp. 5637–5646 (2022)

Moran, S., Marza, P., McDonagh, S., Parisot, S., Slabaugh, G.: Deeplpf: Deep local parametric filters for image enhancement. In: IEEE/CVF Conf. Comput. Vis. Pattern Recognit., pp. 12826–12835 (2020)

Marini, D., Rizzi, A.: A computational approach to color illusions. In: Int. Conf. Image Anal. Process, pp. 62–69 (1997). Springer

Marini, D., Rizzi, A.: A computational approach to color adaptation effects. Image Vis. Comput. **18**(13), 1005–1014 (2000)

Nguyen, C.M., Chan, E.R., Bergman, A.W., Wetzstein, G.: Diffusion in the dark: A diffusion model for low-light text recognition. In: IEEE/CVF Winter Conf. Appl. Comput. Vis., pp. 4146–4157 (2024)

Qian, Y., Kamarainen, J.-K., Nikkanen, J., Matas, J.: On finding gray pixels. In: IEEE/CVF Conf. Comput. Vis. Pattern Recog., pp. 8062–8070 (2019)

Qian, Y., Pertuz, S., Nikkanen, J., Kämäräinen, J.-K., Matas, J.: Revisiting gray pixel for statistical illumination estimation. In: Int. Joint Conf. Comput. Vis. Imag. Comput. Graph. Theory Appl., vol. 4, pp. 36–46 (2018). INSTICC

Rasheed, M.T., Shi, D., Khan, H.: A comprehensive experiment-based review of low-light image enhancement methods and benchmarking low-light image quality assessment. Signal Process. **204**, 108821 (2023)

Shapiro, A., Hedjar, L., Dixon, E., Kitaoka, A.: Kitaoka's tomato: two simple explanations based on information in the stimulus. i-Perception **9**(1), 2041669517749601 (2018)

Shapiro, A., Lu, Z.-L.: Relative brightness in natural images can be accounted for by removing blurry content. Psychological Sci. **22**(11), 1452–1459 (2011)

Serrano-Lozano, D., Arora, A., Herranz, L., Derpanis, K.G., Brown, M.S., Vazquez-Corral, J.: Revisiting image fusion for multi-illuminant white-balance correction. arXiv preprint arXiv:2503.14774 (2025)

Shi, K., Luo, M.R., Rider, A.T., Song, S., Huang, T., Stockman, A.: Individual differences

in color matches and cone spectral sensitivities in 51 young adults. Optics Express **32**, 23597–23616 (2024)

Song, O. A.and Faugeras, Veltz, R.: A neural field model for color perception unifying assimilation and contrast. PLoS Comput. Biol. **15**(6), 1007050 (2019)

Sharma, G., Wu, W., Dalal, E.N.: The CIEDE2000 color-difference formula: Implementation notes, supplementary test data, and mathematical observations. Color Res. Appl. **30**, 21–30 (2005)

Ulucan, O., Ulucan, D., Ebner, M.: BIO-CC: Biologically inspired color constancy. In: Brit. Mach. Vis. Conf. (2022). BMVA Press

Ulucan, O., Ulucan, D., Ebner, M.: Color constancy beyond standard illuminants. In: IEEE Int. Conf. Image Process., pp. 2826–2830 (2022)

Ulucan, O., Ulucan, D., Ebner, M.: Block-based color constancy: The deviation of salient pixels. In: IEEE Int. Conf. Acoust. Speech Signal Process., pp. 1–5 (2023)

Ulucan, O., Ulucan, D., Ebner, M.: Multi-scale block-based color constancy. In: IEEE Eur. Signal Process. Conf., pp. 536–540 (2023)

Ulucan, O., Ulucan, D., Ebner, M.: Multi-scale color constancy based on salient varying local spatial statistics. The Vis. Comput., 1–17 (2023)

Ulucan, O., Ulucan, D., Ebner, M.: A computational model for color assimilation illusions and color constancy. In: Asian Conf. Comput. Vis., pp. 630–647 (2024)

Ulucan, O., Ulucan, D., Ebner, M.: Investigating color illusions from the perspective of computational color constancy. In: Int. Joint Conf. Comput. Vis. Imag. Comput. Graph. Theory Appl. (2024). INSTICC

Ulucan, O., Ulucan, D., Ebner, M.: Revisiting color constancy using cnns: Including recent observations. In: Int. Workshop Comput. Color Imag., pp. 261–273 (2024). Springer

Ulucan, O., Ulucan, D., Ebner, M.: Low-light image enhancement through multi-scale local space average color. In: Eur. Signal Process. Conf., p. (2025). IEEE

Van De Weijer, J., Gevers, T., Gijsenij, A.: Edge-based color constancy. IEEE Trans. Image Process. **16**, 2207–2214 (2007)

Wang, Z., Bovik, A.C., Sheikh, H.R., Simoncelli, E.P.: Image quality assessment: from error visibility to structural similarity. IEEE Trans. Image Process. **13**(4), 600–612 (2004)

Wei, X., Lin, X., Li, Y.: Da-drn: A degradation-aware deep retinex network for low-light image enhancement. Digit. Signal Process. **144**, 104256 (2024)

Wang, W., Wu, X., Yuan, X., Gao, Z.: An experiment-based review of low-light image

enhancement methods. IEEE Access **8**, 87884–87917 (2020)

Wei, C., Wang, W., Yang, W., Liu, J.: Deep retinex decomposition for low-light enhancement. In: Brit. Mach. Vis. Conf., p. (2018)

Wu, W., Weng, J., Zhang, P., Wang, X., Yang, W., Jiang, J.: Uretinex-net: Retinex-based deep unfolding network for low-light image enhancement. In: IEEE/CVF Conf. Comput. Vis. Pattern Recognit., pp. 5901–5910 (2022)

Wang, R., Zhang, Q., Fu, C.-W., Shen, X., Zheng, W.-S., Jia, J.: Underexposed photo enhancement using deep illumination estimation. In: IEEE/CVF Conf. Comput. Vis. Pattern Recognit., pp. 6849–6857 (2019)

Xu, K., Yang, X., Yin, B., Lau, R.W.H.: Learning to restore low-light images via decomposition-and-enhancement. In: IEEE/CVF Conf. Comput. Vis. Pattern Recognit., pp. 2281–2290 (2020)

Yang, S., Ding, M., Wu, Y., Li, Z., Zhang, J.: Implicit neural representation for cooperative low-light image enhancement. In: IEEE/CVF Int. Conf. Comput. Vis., pp. 12918–12927 (2023)

Yucer, K., Kim, C., Sorkine-Hornung, A., Sorkine-Hornung, O.: Depth from gradients in dense light fields for object reconstruction. In: Int. Conf. 3D Vis. (2016). IEEE

Yang, W., Wang, S., Fang, Y., Wang, Y., Liu, J.: From fidelity to perceptual quality: A semi-supervised approach for low-light image enhancement. In: IEEE/CVF Conf. Comput. Vis. Pattern Recognit., pp. 3063–3072 (2020)

Yang, W., Wang, W., Huang, H., Wang, S., Liu, J.: Sparse gradient regularized deep retinex network for robust low-light image enhancement. IEEE Trans. Image Process. **30**, 2072–2086 (2021)

Zeman, A., Brooks, K.R., Ghebreab, S.: An exponential filter model predicts lightness illusions. Frontiers Human Neuroscience **9**, 368 (2015)

Zeki, S.: A Vision of the Brain. Blackwell Science, ISBN: 0632030545, Oxford (1993)

Zhang, X.-S., Gao, S.-B., Li, R.-X., Du, X.-Y., Li, C.-Y., Li, Y.-J.: A retinal mechanism inspired color constancy model. IEEE Trans. Image Process. **25**(3), 1219–1232 (2016)

Zuiderveld, K.: Contrast limited adaptive histogram equalization. Graph. Gems, 474–485 (1994)

Zhang, Y., Zhang, J., Guo, X.: Kindling the darkness: A practical low-light image enhancer. In: ACM Int. Conf. Multimedia, pp. 1632–1640 (2019)